Applied Physics Letters

# All-epitaxial, laterally structured plasmonic materials

Cite as: Appl. Phys. Lett. **120**, 161103 (2022); https://doi.org/10.1063/5.0094677
Submitted: 05 April 2022 • Accepted: 06 April 2022 • Published Online: 20 April 2022

Alec M. Skipper, Priyanka Petluru, Daniel J. Ironside, et al.



Applied Physics Letters ARTICLE scitation.org/journal/apl

# All-epitaxial, laterally structured plasmonic materials

Cite as: Appl. Phys. Lett. **120**, 161103 (2022); doi: 10.1063/5.0094677
Submitted: 5 April 2022 · Accepted: 6 April 2022 ·
Published Online: 20 April 2022



Alec M. Skipper,[a] Priyanka Petluru, Daniel J. Ironside, Ashlee M. García, Aaron J. Muhowski, Daniel Wasserman, and Seth R. Bank

## AFFILIATIONS

Microelectronics Research Center and ECE Department, The University of Texas at Austin, 10100 Burnet Rd., Bldg. 160, Austin, Texas 78758, USA

[a]Author to whom correspondence should be addressed: alecskipper@utexas.edu

## ABSTRACT

Optoelectronic devices in the mid-infrared have attracted significant interest due to numerous potential applications in communications and sensing. Molecular beam epitaxial (MBE) growth of highly doped InAs has emerged as a promising "designer metal" platform for the plasmonic enhancement of mid-infrared devices. However, while typical plasmonic materials can be patterned to engineer strong localized resonances, the lack of lateral control in conventional MBE growth makes it challenging to create similar structures compatible with monolithically grown plasmonic InAs. To this end, we report the growth of highly doped InAs plasmonic ridges for the localized resonant enhancement of mid-IR emitters and absorbers. Furthermore, we demonstrate a method for regaining a planar surface above plasmonic corrugations, creating a pathway to epitaxially integrate these structures into active devices that leverage conventional growth and fabrication techniques.



The mid-infrared wavelength range encompasses atmospheric absorption windows, molecular fingerprints, and blackbody emission, generating significant research interest in mid-infrared devices with wide-ranging applications in free-space communication,[1] medicine,[2,3] and thermal imaging.[4] However, the inherent inefficiencies caused by Auger and Shockley–Read–Hall recombination in semiconductor materials at mid-infrared wavelengths severely degrade optoelectronic device performance. As a result, plasmonic enhancement has emerged as a potential solution for improving the performance of mid-IR optoelectronics.[5,6]

Plasmonics are ideal for overcoming the size and bandwidth limitations of semiconductor optoelectronics due to strong optical field enhancement at the interface of metallic nanostructures that allows for increased light–matter interaction in absorbers and emitters. While plasmonic structures based on noble metals, such as Au and Ag, have shown tremendous promise in enhancing the performance of optoelectronics in the near-IR and visible spectrum,[7–9] noble metals have large negative real permittivity in the mid-IR resulting in weak optical mode confinement.[10] Highly doped semiconductors have emerged as a promising candidate for mid-IR plasmonic materials by acting as "designer metals."[11–13] The small effective mass and high doping level limit of InAs allow for the growth of layers with plasma wavelengths as low as 4.64 $\mu$m.[12,14] By adjusting the doping concentration, the plasma wavelength of molecular beam epitaxy (MBE)-grown InAs can be tailored to a target mid-IR wavelength.[12,13] Furthermore, the low lattice mismatch between InAs and GaSb also allows for the coupling of plasmonic semiconductors with a variety of GaSb-based mid-IR optoelectronic devices.[15,16]

While typical plasmonic materials can be patterned to engineer localized resonances, the lack of lateral control in conventional molecular beam epitaxy makes it challenging to create bottom-up epitaxial plasmonic structures supporting localized plasmonic resonances. Although *ex-situ* patterning of mid-IR plasmonic semiconductors shows great promise in local field enhancement,[17] etched surfaces have proven to be significant sources of carrier recombination in InAs-based optoelectronic devices. Undoped and p-doped InAs interfaces with air experience an accumulation of a charge layer at the surface due to Fermi level pinning.[18,19] This can limit device performance unless steps are taken to passivate the surface.[20–22] A method for producing high-quality laterally structured plasmonic InAs without creating these surface states could allow for higher performance devices and novel device geometries. High field concentrations supported by plasmonic materials have previously been demonstrated to enhance the luminescence and absorption in long-wave infrared III–V emitters

and detectors, respectively.[15,16] By monolithically integrating a semiconductor active region with a highly localized electric field structure, high-efficiency ultrathin devices in traditionally inefficient spectral regions, such as the long-wave infrared, could be developed.

To this end, we have developed an all-MBE process for the growth of embedded mid-IR plasmonic structures for localized field enhancement. We report a three-step growth process that leverages the natural faceting of lateral epitaxial overgrowth techniques to produce corrugated plasmonic InAs nanoridges that can be embedded below a crystalline (001) surface, characterized by structural and optical studies, and confirmed by full wave electromagnetic simulations.

Periodic supply epitaxy (PSE) is a lateral epitaxial overgrowth method that can be tailored to produce {011}-oriented crystal facets above a dielectric mask. PSE was initially developed to enable selective area growth of III–V semiconductors with dielectric masks in MBE[23–25] and was recently utilized in a two-step process to encapsulate amorphous dielectrics in crystalline III–V semiconductor materials through lateral epitaxial overgrowth.[26] Conventional MBE growth conditions were found to be insufficient for selective area epitaxy and lateral epitaxial overgrowth due the formation of polycrystalline deposition on the mask surface.[25] PSE growth suppresses the formation of this polycrystalline deposition by enhancing the desorption and diffusion of group III adatoms on the mask surface. This is primarily achieved by periodically interrupting the group III flux and using elevated growth temperatures to prevent the formation of polycrystalline defects on the $SiO_2$ surface and encourage faceting. Reducing the V/III flux ratio will favorably increase adatom mobility; however, the substrate temperature during PSE growth tends to be the dominant factor with increasing temperature resulting in lower (or even negligible) polycrystalline nucleation. The crystal facet orientation of PSE growth is highly dependent upon the orientation of the underlying dielectric mask. By aligning the dielectric mask with the [010] direction of the semiconductor substrate, PSE produces smooth {011}-oriented lateral growth, which forms a sharp point well-suited for supporting localized resonances. Furthermore, this crystal facet structure can regain a planar (001) crystal surface through an additional continuous growth process.[26]

However, the growth of highly doped InAs requires kinetically limited growth conditions,[13] making it challenging to integrate with the PSE growth process that utilizes high substrate temperatures and low growth rates. To investigate whether faceted plasmonic InAs could be produced by PSE, we performed InAs PSE growth at a substrate temperature of 520 °C, an $As_4$/In flux ratio of 20, and a growth rate of 0.25 $\mu$m/h on [010]-aligned $SiO_2$ templates with and without a Si dopant flux. As seen in Fig. 1, addition of Si during InAs PSE growth results in the formation of polycrystalline deposition on $SiO_2$ and roughening of the lateral overgrowth facets. This is likely caused by a reduction in the group III adatom surface mobility caused by the presence of Si on the surface that has also previously been observed in doped GaAs.[27] Since these defects can act as non-radiative recombination centers that reduce the performance of optoelectronic devices, an alternative approach is needed to produce all-epitaxial localized resonances supported by the plasmonic material.

To address this issue, we developed the three-stage growth process shown schematically in Fig. 2 that uses undoped PSE growth as a template for the growth of corrugated plasmonic InAs. Periodic supply epitaxy of undoped InAs was initiated at a substrate temperature of

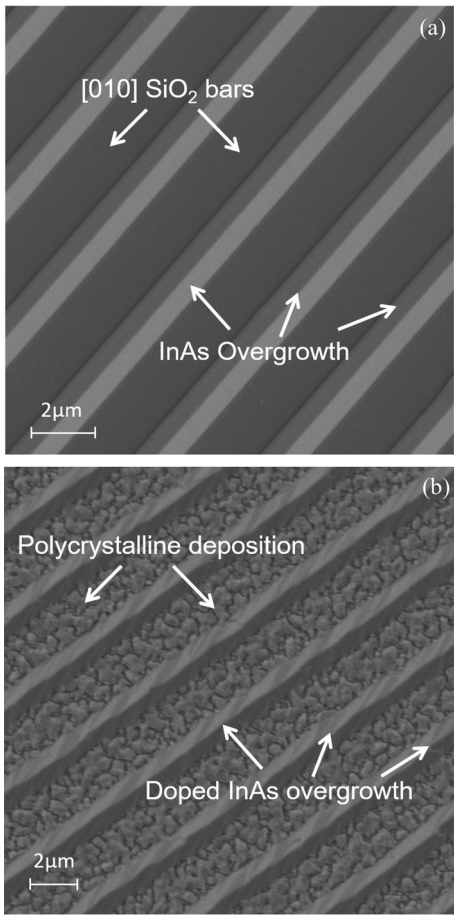


**FIG. 1.** Plan view scanning electron microscope images of PSE-grown InAs (a) without and (b) with high Si doping.

520 °C, an $As_4$/In flux ratio of 20, and a growth rate of 0.25 $\mu$m/h on 25 nm thick [010]-aligned $SiO_2$ templates. $As_4$ is the favored As species for this growth step due its enhanced Ga desorption in comparison to $As_2$.[28,29] This results in the formation of {011}-faceted ridges of undoped InAs seeded from the windows in the $SiO_2$ mask. Since InAs ridges form above the windows, the pitch of the corrugated InAs is set by the pitch of the windows in $SiO_2$. Once the InAs facets meet and completely cover the $SiO_2$ mask, PSE is no longer necessary and the growth conditions can be changed to facilitate the growth of highly n-doped InAs. 500 nm of Si n-doped InAs was grown with conventional continuous MBE at a substrate temperature of 380 °C, an $As_2$/In flux ratio of 1.5, and a growth rate of 0.66 $\mu$m/h. In addition, a Bi flux with an In/Bi flux ratio of 20 was also applied to promote Si dopant incorporation and inhibit surface roughening as described by Wei *et al.*[30] This results in a highly doped plasmonic InAs layer that conforms to the faceted PSE-grown ridges. 2 $\mu$m of undoped InAs was then grown at a substrate temperature of 480 °C, an $As_2$/In flux ratio of 4, and a growth rate of 0.50 $\mu$m/h to embed the plasmonic InAs ridges and return the surface to a planar (001) crystal plane. All samples were grown in an EPI Mod Gen II solid-source molecular beam epitaxy

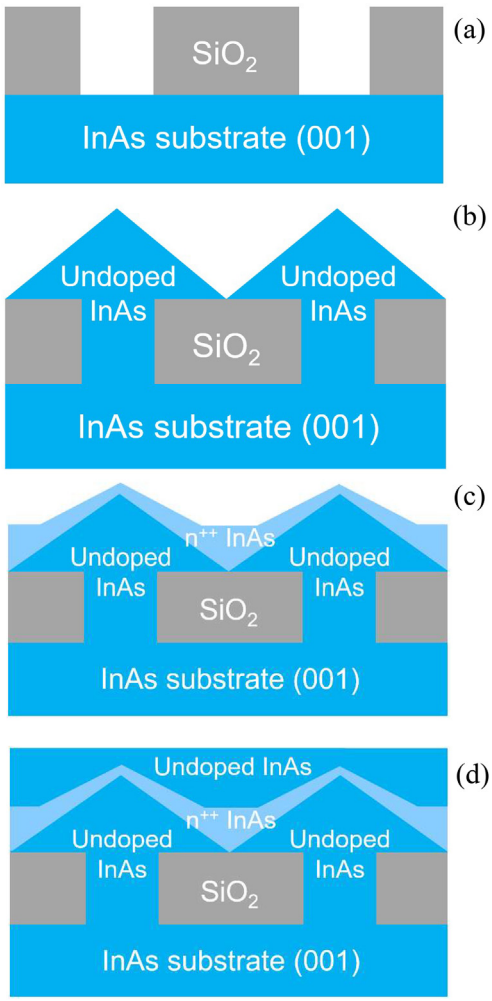


**FIG. 2.** Cross section illustration of the growth process for embedded plasmonic InAs corrugations. (a) $SiO_2$ gratings were patterned along the [010] crystal plane direction of a (001) InAs substrate. (b) Lateral overgrowth of undoped InAs was seeded between the gratings using periodic supply epitaxy. (c) Highly n-type doped InAs was then grown on the faceted undoped InAs features. (d) Finally, undoped InAs was grown to return to a planar (001) surface above the plasmonic corrugations.

system with a Veeco SUMO effusion cell for In, Veeco Mark IV valved As cracker, and an MBE Komponenten silicon sublimation source for Si doping. Switching the arsenic source between $As_4$ and $As_2$ was performed by adjusting the temperature of the arsenic source's cracking zone to 650 and 850 °C, respectively.

Fourier transform infrared spectroscopy (FTIR) and scanning electron microscope (SEM) measurements were performed on the plasmonic InAs corrugations prior to planarization as seen in Fig. 3. FTIR reflection spectra demonstrate that corrugated InAs exhibits a sharp Drude edge similar to planar doped-InAs grown under the same conditions, suggesting that non-planar growth does not compromise plasmonic effects or the suitability of doped-InAs for mid-IR plasmonics. Fitting the reflection data gives a plasma wavelength of 5.2 $\mu$m

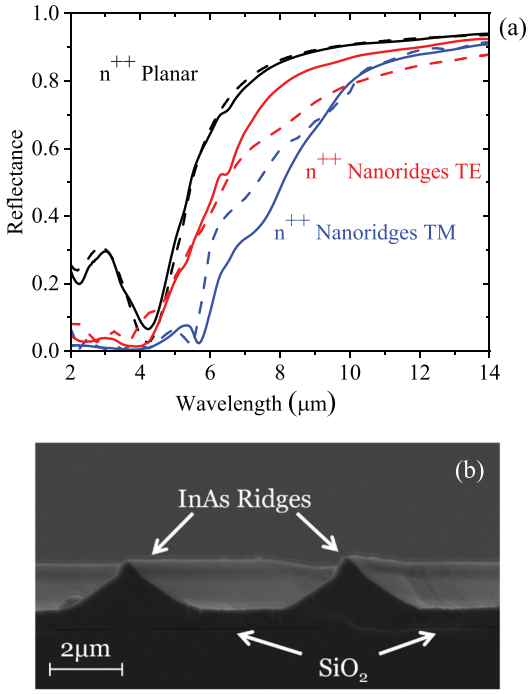


**FIG. 3.** (a) Fourier transform infrared (FTIR) spectroscopy (solid lines) and Drude model fitting (dashed) TE and TM reflection spectra comparing planar plasmonic InAs and 3.0 $\mu$m pitch plasmonic InAs nanoridges. (b) Cross-sectional scanning electron microscope (SEM) images of the InAs corrugations.

and a scattering rate of $2 \times 10^{12}$ Hz. Cross-sectional SEM images confirm that the highly doped InAs converges to a sharp point suitable for high field localization.

The structure of the planar coalescence of the undoped InAs layer above the highly doped corrugations was investigated using atomic force microscopy (AFM) and scanning electron microscopy (SEM). AFM images show a surface roughness as low as 3.8 nm root mean square (RMS), demonstrating that micrometer-scale corrugations of doped InAs can be returned to a planar (001) surface after 2 $\mu$m of undoped InAs growth. This is comparable to the minimum roughness of 3.2 nm RMS observed by Ironside *et al.*[26] after a two-step PSE and planarization and growth process with undoped materials. This suggests that addition of the highly doped InAs layer does not adversely affect the ability to restore a planar surface. Cross-sectional SEM images show a clear contrast between the highly doped and undoped InAs. The angle and thickness of these layers can be used to simulate and design structures for use with active devices. The planar encapsulation of the plasmonic InAs corrugations ensures compatibility with conventional growth and fabrication techniques performed on (001) substrates.

The optical response of our structured plasmonic materials was simulated using the wave optics module in COMSOL Multiphysics finite element method software. The doped semiconductor was modeled using the Drude approximation with permittivity

$$\varepsilon(\omega) = \varepsilon_\infty \left(1 - \frac{\omega_p^2}{\omega^2 + i\gamma\omega}\right), \quad \omega_p^2 = \frac{Ne^2}{\varepsilon_\infty \varepsilon_o m^*},$$

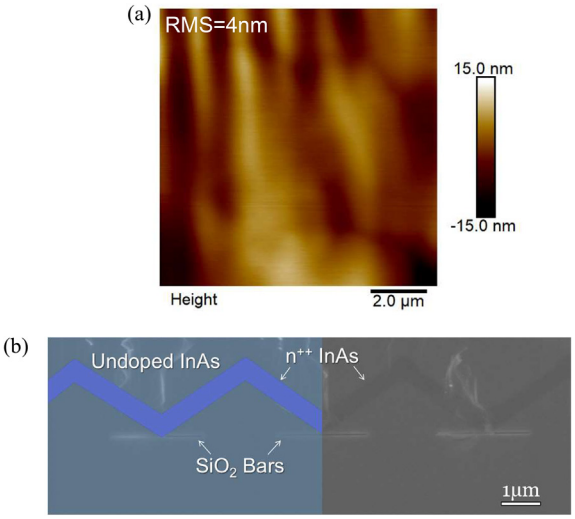


**FIG. 4.** (a) Atomic force microscope (AFM) image of the planarized plasmonic InAs corrugations showing that the (001) crystal surface has been recovered to a roughness of 4 nm RMS over a 10 × 10 $\mu m^2$ area. (b) Cross-sectional scanning electron microscope (SEM) image of the planarized plasmonic InAs corrugations.

where $\varepsilon_\infty$ is the dielectric background permittivity of InAs ($\varepsilon_\infty = 12.3$), $\gamma$ is the free carrier scattering time, and $\omega_p$ is the plasma frequency (corresponding to the frequency associated with epsilon-near-zero response). The reflection spectra from the un-patterned, planar, and portion of each wafer are collected and then modeled in COMSOL with fitting parameters of the plasma wavelength ($\lambda_p = \frac{2\pi c}{\omega_p}$) and scattering time ($\gamma$). For highly doped semiconductors, the plasma wavelength effectively tunes the spectral position of the sharp rise of reflectivity, while the scattering time controls the slope of the rising edge in reflectivity. The relative independence of the two fitting parameters allows for a unique combination of ($\lambda_p, \gamma$) for each of the films investigated. Using this approach, we extract $\lambda_p = 5.2\ \mu m$ and $\gamma = 4 \times 10^{12}$ Hz for the $n^{++}$ layer in the unplanarized growth and $\lambda_p = 5.75\ \mu m$ and $\gamma = 2x10^{12}$ Hz for the $n^{++}$ layer in the planarized growth. The simulated reflection for each of the samples uses the extracted permittivity for the $n^{++}$ layers and the permittivity of the undoped InAs[31] and $SiO_2$[32] layers from the literature. The n-type InAs substrate is treated as a more lightly doped version of the epitaxially grown $n^{++}$ InAs with $\lambda_p = 40\ \mu m$ and $\gamma < 10^{10}$ Hz (which has minimal effect on the simulated optical response). The simulated geometries of the two samples are extracted from the cross-sectional SEMs shown in Figs. 3(b) and 4(b). In order to accurately model the incident light in our experimental mid-IR microscope setup, the simulated

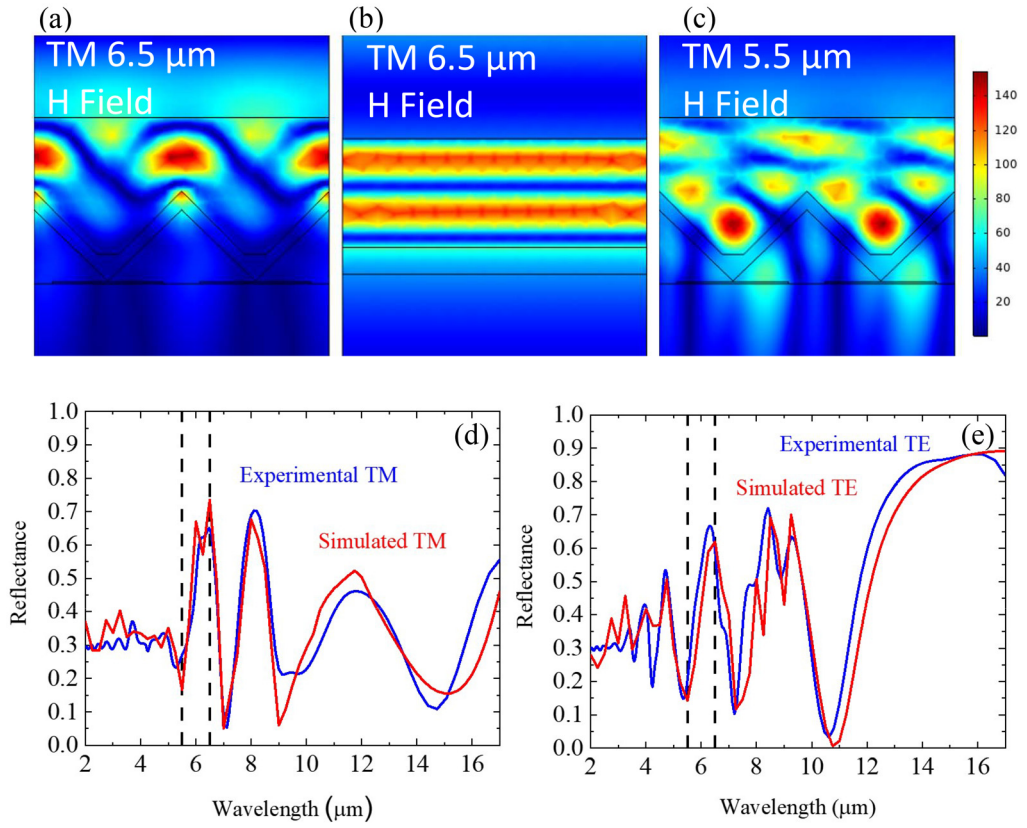


**FIG. 5.** Finite element model of the electric field intensity with 6.5 $\mu m$ TM light incident on (a) 2.8 $\mu m$ pitch planarized InAs corrugations and (b) planar highly doped InAs. This demonstrates localized electric field enhancement at the tips of the corrugations.(c) Finite element model of the magnetic field intensity with 5.5 $\mu m$ TM light incident on 2.8 $\mu m$ pitch planarized InAs corrugations. Experimental and simulated reflectance spectra of the same structure under (d) TM and (e) TE illumination.

reflectance data were the average of light from two incident directions using a 3D model. The elevation angle of incidence in both cases was set to 18°, while the azimuth angles of incidence were set to 0° and 90°.

Finite element modeling of the fully planarized structure demonstrates the strong electric field localization effects of the corrugated plasmonic InAs. As seen in Fig. 5(a), under TM illumination at 6.5 $\mu$m, the electric field exhibits the maximum intensity at the peak of the triangular highly doped InAs corrugations. The interface between the metal-like doped InAs and dielectric-like undoped InAs leads to plasmonic enhancement of the electric field that is strongly localized to the tapered point of the faceted material. This stands in sharp contrast to the planar highly doped InAs material modeled in Fig. 5(b). While the electric field intensity is enhanced near the interface between planar doped InAs and undoped InAs, there is no localized resonant enhancement due to the lack of a defined sub-wavelength geometric feature.

The addition of a planarizing layer of undoped InAs above the plasmonic corrugations complicates the reflection spectrum due to cavity resonances between the faceted highly doped corrugations and the planar top surface. As seen in Fig. 5(c), optical modes at wavelengths shorter than the plasma wavelength of the $n^{++}$ InAs can be confined in the valleys of the undoped overgrown InAs corrugations above the $SiO_2$ mask, a result of the index contrast between the dielectric and doped semiconductor material. The red shift of the plasma wavelength from the unplanarized structure to the planarized structure is likely due to annealing of the highly doped layer during the higher temperature growth of the undoped planarization layer. Simulated reflection spectra match well to experimental spectra measured using FTIR. This suggests that embedded highly doped InAs structures can be engineered to exploit resonances in the valleys of the corrugations in addition to the peaks. While this localized field enhancement is not plasmonic, it shows great promise for the enhancement of site selective quantum emitters. Patterned trenches and holes have previously been used to control the nucleation sites of III–V quantum dots.[33,34] By using the trenches formed from the lateral overgrowth process to localize quantum dots into positions of the high field intensity, individual quantum emitters could see strong efficiency enhancements.

In conclusion, we have demonstrated an all-epitaxial method for the growth of plasmonic materials supporting localized resonance in the mid-IR. By combining lateral epitaxial overgrowth techniques with recent advances in highly Si-doped InAs, we developed a three-stage growth approach that results in the planar encapsulation of corrugated metallic InAs. Optical characterization and modeling demonstrate the potential of these structures for plasmonic enhancement of mid-IR optoelectronics due their strong localized field enhancement effects. The ability to incorporate corrugated structures below a planar surface enables integration with conventional planar growth and processing techniques. The use of highly doped InAs as a designer metal enables the tuning of the plasma wavelength, allowing these structures to be engineered for the desired mid-IR wavelength. Looking forward, these structures can be integrated with site-controlled quantum dots or ultra-thin type II superlattices to create high-efficiency mid-IR optoelectronic devices. The monolithic integration of these localized field enhancement structures represents a major step toward addressing the long-standing challenges of enhancing optoelectronic device performance in the mid-IR.

This research was partially supported by the National Science Foundation through the Center for Dynamics and Control of Materials: an NSF Materials Research Science and Engineering Center (MRSEC) under Cooperative Agreement No. DMR-1720595, as well as Nos. DMR-1839175 and ECCS-1926187. This work was performed in part at the University of Texas Microelectronics Research Center, a member of the National Nanotechnology Coordinated Infrastructure (NNCI), which was supported by the National Science Foundation (Grant No. ECCS-1542159).

## AUTHOR DECLARATIONS

### Conflict of Interest

The authors have no conflicts to disclose.

## DATA AVAILABILITY

The data that support the findings of this study are available from the corresponding author upon reasonable request.

## REFERENCES

[1]R. Martini, C. Bethea, F. Capasso, C. Gmachl, R. Paiella, E. A. Whittaker, H. Y. Hwang, D. L. Sivco, J. N. Baillargeon, and A. Y. Cho, "Free-space optical transmission of multimedia satellite data streams using mid-infrared quantum cascade lasers," Electron. Lett. **38**, 181–183 (2002).
[2]W. Petrich, "Mid-infrared and raman spectroscopy for medical diagnostics," Appl. Spectrosc. Rev. **36**, 181–237 (2001).
[3]F. K. Tittel, D. Richter, and A. Fried, "Mid-infrared laser applications in spectroscopy," in *Solid-State Mid-Infrared Laser Sources*, Topics in Applied Physics Vol. 89, edited by I. T. Sorokina and K. L. Vodopyanov (Springer, Berlin, Heidelberg, 2003).
[4]M. Vollmer and K.-P. Möllmann, *Infrared Thermal Imaging: Fundamentals, Research and Applications* (John Wiley & Sons, 2017).
[5]R. Stanley, "Plasmonics in the mid-infrared," Nat. Photonics **6**, 409–411 (2012).
[6]S. Law, V. Podolskiy, and D. Wasserman, "Towards nano-scale photonics with micro-scale photons: The opportunities and challenges of mid-infrared plasmonics," Nanophotonics **2**, 103–130 (2013).
[7]T. Echtermeyer, L. Britnell, P. Jasnos, A. Lombardo, R. Gorbachev, A. Grigorenko, A. Geim, A. C. Ferrari, and K. Novoselov, "Strong plasmonic enhancement of photovoltage in graphene," Nat. Commun. **2**, 458 (2011).
[8]M. Heo, H. Cho, J.-W. Jung, J.-R. Jeong, S. Park, and J. Y. Kim, "High-performance organic optoelectronic devices enhanced by surface plasmon resonance," Adv. Mater. **23**, 5689–5693 (2011).
[9]M.-K. Kwon, J.-Y. Kim, B.-H. Kim, I.-K. Park, C.-Y. Cho, C. C. Byeon, and S.-J. Park, "Surface-plasmon-enhanced light-emitting diodes," Adv. Mater. **20**, 1253–1257 (2008).
[10]M. A. Ordal, R. J. Bell, J. Alexander, R. W. L. L. Long, and M. R. Querry, "Optical properties of fourteen metals in the infrared and far infrared: Al, Co, Cu, Au, Fe, Pb, Mo, Ni, Pd, Pt, Ag, Ti, V, and W," Appl. Opt. **24**, 4493–4499 (1985).
[11]M. Shahzad, G. Medhi, R. E. Peale, W. R. Buchwald, J. W. Cleary, R. Soref, G. D. Boreman, and O. Edwards, "Infrared surface plasmons on heavily doped silicon," J. Appl. Phys. **110**, 123105 (2011).
[12]S. Law, D. C. Adams, A. M. Taylor, and D. Wasserman, "Mid-infrared designer metals," Opt. Express **20**, 12155–12165 (2012).
[13]S. Law, L. Yu, and D. Wasserman, "Epitaxial growth of engineered metals for mid-infrared plasmonics," J. Vac. Sci. Technol. B **31**, 03C121 (2013).
[14]M. Desouky, A. Mahmoud, and M. Swillam, "Tunable mid IR focusing in InAs based semiconductor hyperbolic metamaterial," Sci. Rep. **7**, 15312 (2017).
[15]L. Nordin, K. Li, A. Briggs, E. Simmons, S. R. Bank, V. A. Podolskiy, and D. Wasserman, "Enhanced emission from ultra-thin long wavelength infrared superlattices on epitaxial plasmonic materials," Appl. Phys. Lett. **116**, 021102 (2020).

[16]L. Nordin, P. Petluru, A. Kamboj, A. J. Muhowski, and D. Wasserman, "Ultra-thin all-epitaxial plasmonic detectors," arXiv:2107.04143 (2021).
[17]V. N'Tsame Guilengui, L. Cerutti, J.-B. Rodriguez, E. Tournié, and T. Taliercio, "Localized surface plasmon resonances in highly doped semiconductor nanostructures," Appl. Phys. Lett. **101**, 161113 (2012).
[18]C. A. Mead and W. G. Spitzer, "Fermi level position at semiconductor surfaces," Phys. Rev. Lett. **10**, 471–472 (1963).
[19]L. O. Olsson, C. B. M. Andersson, M. C. Håkansson, J. Kanski, L. Ilver, and U. O. Karlsson, "Charge accumulation at InAs surfaces," Phys. Rev. Lett. **76**, 3626–3629 (1996).
[20]M. J. Kane, G. Braithwaite, M. T. Emeny, D. Lee, T. Martin, and D. R. Wright, "Bulk and surface recombination in InAs/$AlAs_{0.16}Sb_{0.84}$ 3.45 $\mu$m light emitting diodes," Appl. Phys. Lett. **76**, 943–945 (2000).
[21]A. Gin, Y. Wei, J. Bae, A. Hood, J. Nah, and M. Razeghi, "Passivation of type II InAs/GaSb superlattice photodiodes," in Proceedings of the 30th International Conference on Metallurgical Coatings and Thin Films [Thin Solid Films **447–448**, 489–492 (2004)].
[22]A. Gin, Y. Wei, A. Hood, A. Bajowala, V. Yazdanpanah, M. Razeghi, and M. Tidrow, "Ammonium sulfide passivation of type-II InAs/GaSb superlattice photodiodes," Appl. Phys. Lett. **84**, 2037–2039 (2004).
[23]F. Allegretti and T. Nishinaga, "Periodic supply epitaxy: A new approach for the selective area growth of GaAs by molecular beam epitaxy," J. Cryst. Growth **156**, 1–10 (1995).
[24]G. Bacchin and T. Nishinaga, "Fabrication of submicrometer structures by PSE/MBE," J. Cryst. Growth **211**, 389–394 (2000).
[25]T. Nishinaga and G. Bacchin, "Selective area MBE of GaAs, alas and their alloys by periodic supply epitaxy," Thin Solid Films **367**, 6–12 (2000).
[26]D. J. Ironside, A. M. Skipper, T. A. Leonard, M. Radulaski, T. Sarmiento, P. Dhingra, M. L. Lee, J. Vuckovic, and S. R. Bank, "High-quality GaAs planar coalescence over embedded dielectric microstructures using an All-MBE approach," Cryst. Growth Des. **19**, 3085–3091 (2019).
[27]L. Däweritz, K. Hagenstein, and P. Schützendübe, "Si incorporation during molecular beam epitaxy growth of GaAs and preferential attachment of Si atoms at misorientation steps," J. Vac. Sci. Technol. A **11**, 1802–1806 (1993).
[28]E. M. Gibson, C. T. Foxon, J. Zhang, and B. A. Joyce, "Gallium desorption from GaAs and (Al,Ga)As during molecular beam epitaxy growth at high temperatures," Appl. Phys. Lett. **57**, 1203–1205 (1990).
[29]T. Ogura and T. Nishinaga, "Efficiency difference in Ga adatom incorporation in MBE growth of GaAs with $As_2$ and $As_4$ molecular beams," J. Cryst. Growth **211**, 416–420 (2000).
[30]D. Wei, S. Maddox, P. Sohr, S. Bank, and S. Law, "Enlarged growth window for plasmonic silicon-doped InAs using a bisumuth surfactant," Opt. Mater. Express **10**, 302–311 (2020).
[31]O. G. Lorimor and W. G. Spitzer, "Infrared refractive index and absorption of InAs and CdTe," J. Appl. Phys. **36**, 1841–1844 (1965).
[32]J. Kischkat, S. Peters, B. Gruska, M. Semtsiv, M. Chashnikova, M. Klinkmüller, O. Fedosenko, S. Machulik, A. Aleksandrova, G. Monastyrskyi, Y. Flores, and W. T. Masselink, "Mid-infrared optical properties of thin films of aluminum oxide, titanium dioxide, silicon dioxide, aluminum nitride, and silicon nitride," Appl. Opt. **51**, 6789–6798 (2012).
[33]S. Kiravittaya, H. Heidemeyer, and O. Schmidt, "Growth of three-dimensional quantum dot crystals on patterned GaAs (001) substrates," in Proceedings of the Fifth International Workshop on Epitaxial Semiconductors on Patterned Substrates and Novel Index Surfaces (ESPS-NIS) [Physica E **23**, 253–259 (2004)].
[34]Z. M. Wang, J. H. Lee, B. L. Liang, W. T. Black, V. P. Kunets, Y. I. Mazur, and G. J. Salamo, "Localized formation of InAs quantum dots on shallow-patterned GaAs (100)," Appl. Phys. Lett. **88**, 233102 (2006).